A mmW Broadband Dual-Polarized Dielectric Resonator Antenna Based on Hybrid Modes

Jerzy Kowalewski ⓘ, *Member, IEEE*, Joerg Eisenbeis ⓘ, *Student Member, IEEE*, Alisa Jauch ⓘ,
Jonathan Mayer ⓘ, *Student Member, IEEE*, Marius Kretschmann ⓘ, and Thomas Zwick ⓘ, *Fellow, IEEE*

Abstract—This letter presents a dual-polarized dielectric resonator antenna (DRA) achieving more than 40% fractional bandwidth, thus the 5G bands n257 and n260 are covered with a single antenna. Hence, the system cost is considerably reduced, since only one antenna array system is required. The bandwidth could be reached thanks to the wideband monopoles and differential feeding enabling hybrid operation in monopole and DRA mode. The antenna uses a standard two metal layer printed-circuit-board (PCB) process and 3-D printing for the fabrication of the dielectric resonators, reducing the number of PCB layers and the overall production cost. The prototypes of a single element and 2×2 array show a maximal gain of 7.1 and 10.4 dBi, respectively.

Index Terms—Antenna array, dielectric resonator antennas, millimeter-wave (mmW) technology, 5G, 3-D printing.

I. INTRODUCTION

AS AN answer to the tremendous growth in data traffic, big parts of the 5G communication will be moved to the available frequency bands in millimeter wave (mmW) range [1]. Only this way, wide band channels can be reserved for growing numbers of mobile equipment users. Additionally the reliability of links should be increased and latency should decrease. Hence, the Third Generation Partnership Project (3GPP) has defined the n257 band from 26.5 to 29.5 GHz and the n260 band from 37 to 40 GHz [2]. To ensure the quality of huge number of mobile connections simultaneously and battle the severe path loss in mmW range massive multiple-input–multiple-output (mMIMO) antenna systems will be used [3]. The shift to higher frequencies enables the reduction of overall antenna array's size as well as miniaturization of the RF front-ends [4]. At the same time fulfilling the bandwidth and price requirements with the conventional antennas becomes challenging. Furthermore, those antennas have to support dual polarization to further increase the communication data rate [2]. Thus, new antenna concepts should be developed.

The antennas presented in the literature are mostly based on the printed circuit board (PCB) process. However, conventional microstrip patch antennas [5] or substrate integrated waveguide (SIW) antennas [6] using a single substrate layer can only achieve up to 10% fractional bandwidth. Higher bandwidths exceeding 20% can be achieved by using a parasitic patch antenna concept [7]. This solution can also be applied for dual-band designs [8], [9]. In this case, a multilayer PCB process is required. A promising concept to improve the bandwidth without increasing the number of PCB layers are dielectric resonator antennas (DRAs) [10]. Different techniques to increase the bandwith of circular polarized DRAs were presented in the literature [11]–[14]. Among wideband linear polarized DRAs [15]–[17], differential feeding is a promising approach, as 30% bandwidth can be achieved. Nonetheless, designs [11], [14], [16] use complicated feeding networks. Thus, a different feeding structure is required to achieve a low complex design.

This letter introduces a novel feeding structure for wide-band dual-polarized DRAs. The proposed feeding concept enables a hybrid operation in slot and DRA mode, hence, broadband performance is achieved. Section II presents the design and optimization of the feeding structure and choice of the resonator. The array design is presented in Section III, while the measurement results of the fabricated prototypes are shown in Section IV.

II. ANTENNA DESIGN

Dielectric resonator antennas can be excited in various ways including probes, microstrip line feed, and aperture coupling [10]. These methods are, however, limited in bandwidth [18], [19]. Thus, a wideband feed is required to support fractional bandwidth above 30%. In [20], a slot antenna for ultrawideband applications was introduced. In this letter, it is proposed to use a similar structure as an excitation of DRA. The feeding structure consists of a circular slot and four elliptical monopole elements placed on x- and y-axes (see Fig. 1). The elliptical shape was chosen for wideband performance. The monopoles are fed pairwise with $180°$ phase shift. As a result, a current distribution similar to two parallel dipole antennas is obtained. These dipoles are exciting the slot, and thus, it is the radiating element. Therefore, the diameter of the circular slot defines the lower cutoff frequency of the antenna. The slot diameter is set to 2.84 mm, and corresponds to half a wavelength at 26.5 GHz if an ε_r of 4.5 for the Preperm L450 resonator material and ε_r of 3.38 for the Rogers 4003 substrate are considered.

A. Feeding Structure

The feeding network is placed on a 0.203 mm thick Rogers 4003 substrate. The elliptical elements are 0.8 mm in length and 0.27 mm in width (see Fig. 1). This slender form was chosen
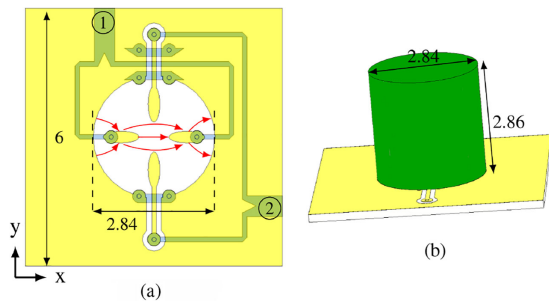
Fig. 1. Layout of the antenna feeding structure on the PCB and perspective view of the antenna. Yellow color represents top, while blue the bottom metal layer. Red arrows represent the E-field. Dimensions are given in millimeters. (a) Final layout. (b) Perspective view.
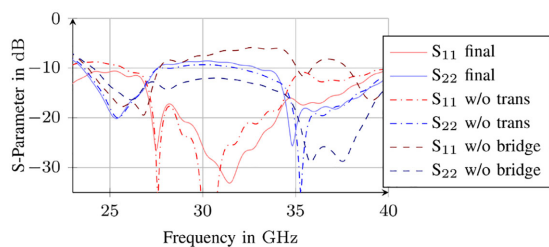

Fig. 2. Simulated *S*-parameters of the dual-polarized antenna element. Ports 1 and 2 correspond with horizontal and vertical polarization, respectively.

to fit the impedance of 100 Ω feeding lines. The monopole pairs are fed using 100 Ω lines, simple T-junction and a 50 Ω line. One of the 100 Ω lines is longer to introduce the required 180° phase shift. A triangle was cut away from the T-junction as well as chamfered corners were used to improve the return loss (see Fig. 1). The elliptical elements and the ground plane are placed on the top metal layer, while the feeding network is placed mostly on the bottom layer. However, to enable feeding of both polarizations with only two metal layers, a part of the network for horizontal polarization is placed on the top layer. Thus, the vertical monopoles are fed with coplanar waveguide (CPW) lines connected by a via to microstrip line on the bottom layer. This transition was simultaneously used as a 90° bend. However, an interruption in the circular slot appears due to the use of CPW. As a result, the radiation parameters and matching for the horizontal elements deteriorate (see Fig. 2). To solve this problem, a bridge structure consisting of two vias and a line on the bottom metal layer is used. An important part of the feeding network is the intersection between transmission lines feeding different polarizations. Gaps between the signal line and ground of a CPW are required for its proper function. However, these gaps are causing interruption in the ground plane of the microstrip line on the bottom metal layer. In order to allow proper operation of the transmission line, a microstrip to CPW to microstrip transition was established at this place (see Fig. 1). The ground lines of the CPW are connected to the antenna ground plane using vias. These lines are tapered at the parts facing the microstrip line to enable proper transition. Introducing this transition improved the matching for port 1 in the lower and upper part (above 35 GHz) of the antenna operation band (see Fig. 2). At the same time, the matching for port 2 deteriorates slightly by around 0.5 dB.

TABLE I
GAIN OF THE PROPOSED DRA OVER THE FREQUENCY BAND

Port	Frequency in GHz				
	25	28	30	35	38
1	5.3 dBi	6.2 dBi	6.8 dBi	7.2 dBi	7.4 dBi
2	6 dBi	6.2 dBi	6.5 dBi	6.7 dBi	6.9 dBi

B. Dielectric Resonator

In this letter, a cylindrical dielectric resonator is chosen as a radiating element (see Fig. 1). The dielectric material used is an acrylonitrile butadiene styrene (ABS)-based Preperm L450 with ε_r of 4.5. The loss tangent given by the manufacturer is 0.004 at 2.4 GHz, while the measurements, using an open-ended coaxial probe, done at our institute show 0.02 at 28 GHz. This material was selected due to relatively low dielectric constant, thus leading to higher radiation efficiency and a low quality factor Q of the resonator. As a result increased bandwidth is achieved. Furthermore, it is commercially available as a filament for fused deposition modeling (FDM) 3-D printing, enabling cheap in-house prototyping. Considering the used feeding method and its position, the electric field is coupled to the resonator and the HEM_{11} mode is excited. The details of the coupling theory are given in [21]. This mode provides the maximum radiation in a broadside direction and it is excited starting from around 30 GHz. Dimensions of the cylindrical resonator were approximated using equation given in [21]. The diameter and height of the resonator are 2.84 and 2.86 mm, respectively. Below 30 GHz, the radiation comes from monopoles in the feeding structure and the dielectric resonator works more as a director increasing the gain in the desired direction.

C. Simulation Results

The optimized DRA, as presented in Fig. 1, was finally evaluated in terms of return loss, isolation, and gain. In the frequency range from 23 to 40 GHz the return loss is better than 9.5 dB (voltage standing wave ratio of 2) for both antenna ports. The isolation between the antenna ports is better than 12 dB within this band. The gain varies between 5.3 and 7.4 dBi (see Table I) and slightly exceeds the gain achieved by patch antennas presented in [5] and [8]. Since the construction of the feeding structure is not perfectly rotation symmetric, differences in gain between horizontal and vertical polarization (ports 1 and 2) can be observed.

III. ARRAY DESIGN

Due to high path loss in mmW range, the antennas are used as elements of arrays. Thus, a 2×2 array with a fixed beam is designed, to demonstrate the functionality of the proposed arrangement. The array elements are separated by 7.5 mm. This distance corresponds with $0.7\lambda_0$ at 28 GHz and $0.96\lambda_0$ at 38.5 GHz (λ_0 represents the free space wavelength), which are the center frequencies of the n257 and the n260 band. This distance was chosen to fit the transmission lines of the feeding network between antenna elements. However, this distance is bigger than normally used $0.6\lambda_0$, it is smaller than λ_0 in the higher frequency band, thus grating lobes can be avoided.

The feeding network consists only of 50 and 100 Ω microstrip lines, which are 0.484 and 0.105 mm in width, respectively. The 100 Ω line almost reaches the fabrication limit, which is
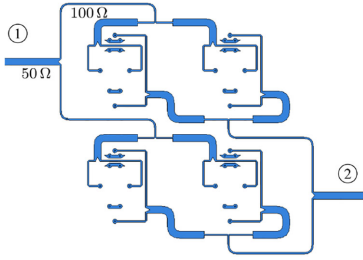
Fig. 3. Layout of the 2 × 2 array feeding network.

TABLE II
GAIN OF THE PROPOSED 2 × 2 DRA ARRAY OVER THE FREQUENCY BAND

| Port | Frequency in GHz | | | | |
	25	28	30	35	38
1	9.9 dBi	11 dBi	11.5 dBi	10.6 dBi	9.6 dBi
2	9.8 dBi	10.1 dBi	12 dBi	9.4 dBi	8.9 dBi

0.1 mm for most of the commercially available PCB production processes. The 50 Ω lines are routed from the ports of single antenna elements toward T-junctions combining the signals from antenna pairs (see Fig. 3). Between each T-junction and a 50 Ω line, a quarter-wave impedance transformer is placed. A 0.25λ (at 33 GHz) long section of 100 Ω line transforms 50 Ω into 200 Ω required at the input of the T-junction. From these T-junctions, 100 Ω lines are routed to the next stage T-junction combining the antenna pairs to one common 50 Ω port for four elements (see Fig. 3). For 90° turns, line arc bends were used to omit additional losses.

The array shows return loss better than 8 dB between 23 and 40 GHz. The worst performance is observed at around 28 and 40 GHz for port 2. The isolation is better than 13 dB in the whole frequency band. The simulated gain of the array varies between 8.9 and 12 dBi (see Table II). Even if around 0.5 dB losses in the feeding network is considered, some of the values are lower than the theoretically expected ones by up to 3.5 dB, e.g., port 2 at 38 GHz. This is due to the narrow-band character of the quarter-wave impedance transformer used in the network. Additionally, these results could be expected from the return loss analysis.

IV. PROTOTYPE FABRICATION AND MEASUREMENT

Finally, two prototypes were fabricated, one of the single DRA element and one of the 2 × 2 DRA array. The PCBs were chemically etched and galvanized with a gold layer by a commercial company. In order to reduce the influence of the used connectors on the radiation pattern measurements, the antennas were placed in the center of a 56 × 56 mm board (see Fig. 4). Two 2.92 mm coaxial connectors from Cinch Connectivity Solutions were used. The cylindrical radiating elements are printed using an Ultimaker 3 Extended 3-D printer and manually attached to the PCBs using Loctite 406 adhesive.

The measurement of the S-parameters of the single element shows, that at some points of the desired band of operation, the return loss at port 1 reaches only 8 dB [see Fig. 5(a)]. This value is around 1.5 dB worse than expected from simulation. Additionally, a ripple caused by a standing wave between the connector and T-junction can be observed. The return loss at port
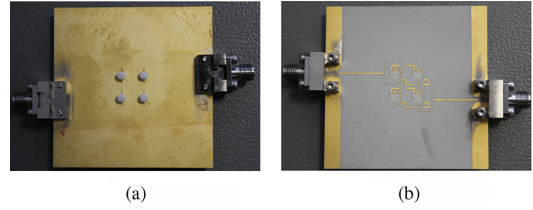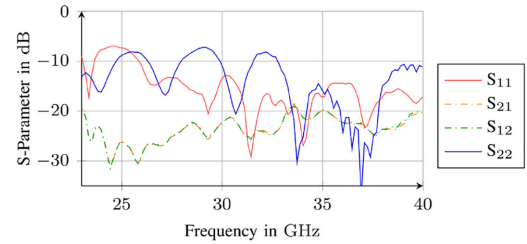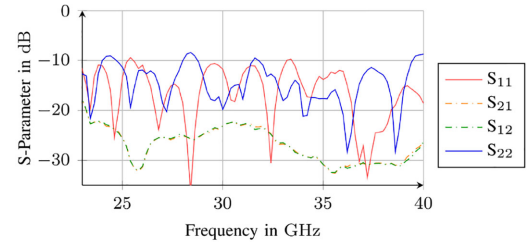

Fig. 4. Fabricated prototype of the dual-polarized 2 × 2 DRA array. (a) Top view. (b) Bottom view.

(a)

(b)

Fig. 5. Measured S-parameters of the fabricated prototypes. Ports 1 and 2 correspond with horizontal and vertical polarization, respectively. (a) Single DRA. (b) 2 × 2 DRA array.
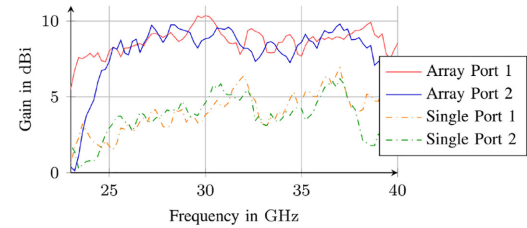

Fig. 6. Measured maximal gain of the 2 × 2 DRA array and single DRA. Ports 1 and 2 correspond with horizontal and vertical polarization, respectively.

2 is better than 12 dB between 26.5 and 40 GHz. The isolation between the antenna ports is better than 19 dB. Considering the 2 × 2 DRA array, return loss better than 9 dB within the whole band for both ports (see Fig. 5). The isolation is better than 23 dB. The worst performance is observed at around 28 and 40 GHz for port 2, which was also the case for simulation results.

In the next step, the fabricated prototypes were measured in an anechoic chamber. Considering the single element DRA, a maximal gain of 7.1 dBi is observed for port 1 at 36.9 GHz, while maximal gain for the port 2 is 6.8 dBi at 36.8 GHz (see Fig. 6). The measured gain in the lower part of antenna's operational band is lower by about 2 dB than expected from
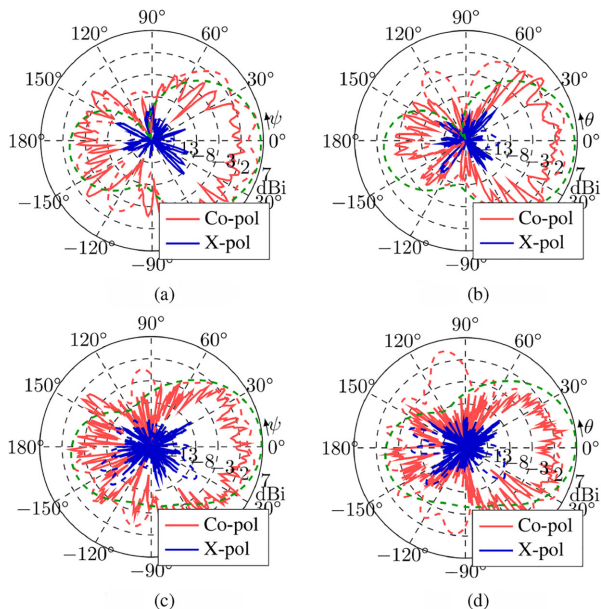
Fig. 7. Gain of the single DRA element in the E-plane. Solid lines represent measured and dashed lines simulated results. Green line represents the simulation results without connectors. (a) Port 1, 28 GHz. (b) Port 2, 28 GHz. (c) Port 1, 38 GHz. (d) Port 2, 38 GHz.

Fig. 8. Gain of the 2×2 DRA array in the E-plane. Solid lines represent measured and dashed lines simulated results. Green line represents the simulation results without connectors. (a) Port 1, 28 GHz. (b) Port 2, 28 GHz. (c) Port 1, 38 GHz. (d) Port 2, 38 GHz.

TABLE III
COMPARISONS OF DIFFERENT DUAL-POLARIZED ANTENNAS

	[8]	[15]	[18]	[19]	this work
BW (%)	6	30	2.6	7.9	42
Isolation (dB)	15	37	18	36	20
Gain (dBi)	4	9.4	-	6.8	6.1
X-pol (dB)	−20	−20	−13	−34	−15
Size (λ^2)	0.25	0.25	0.04	1	0.43
Height (λ)	0.08	0.44	0.05	0.2	0.33

simulation, while in the higher frequency range, the simulated values could be nearly achieved. In general, the main beam is rippled and half-power beamwidth increases due to bigger antenna board and metallic connectors that are of considerable size compared to the structure (see Fig. 7). The ripples are especially visible in the lower frequency range (see Fig. 7) what might explain lower gain. Additionally, differences between E-plane radiation pattern for horizontal and vertical polarization (ports 1 and 2) can be observed. There is more radiation in the angular range from $60°$ to $90°$ for horizontal polarization due to the connectors [see Fig. 7(a)]. These results correspond well with the simulation of whole prototype. In the whole frequency range, the cross-polarization level is lower than $−15$ dB.

Considering the 2×2 DRA array, a maximal gain of 10.4 dBi is observed for port 1 at 30 GHz (see Fig. 6). This value is smaller than the simulated gain for this frequency by only 1 dB. The maximal gain for the port 2 is 10.1 dBi at 36.8 GHz. The measured gain in the frequency range between 26.5 and 40 GHz has values between 7.6 and 10.4 dBi for both polarizations. As can be expected from the discussion in Section III, the sidelobe level increases in higher part of the frequency band, due to element spacing (see Fig. 8). Furthermore, the side lobes are higher in the E-plane of the horizontal polarization [see Fig. 8(a)] than in the case of vertical polarization [see Fig. 8(b)]. It is once again due to the connectors. The cross-polarization level is lower
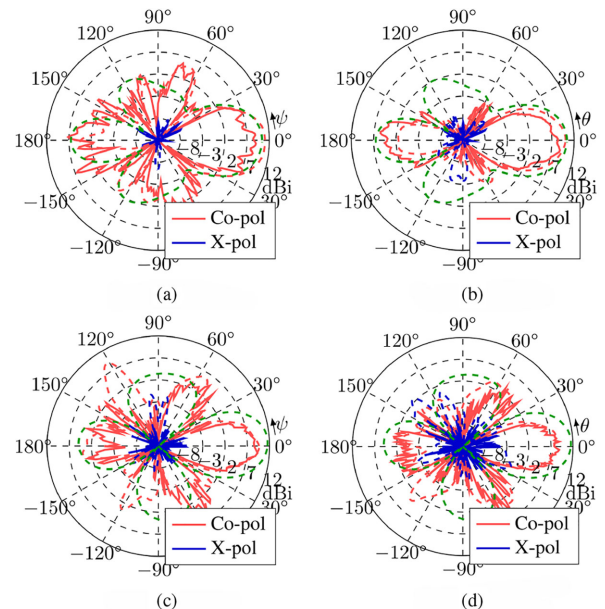
than $−12$ dB in the whole frequency range. The simulated total efficiency for a single element is better than 90%, while the array efficiency lies between 71% and 86%. Considering the measured radiation patterns, which show a slightly reduced gain compared to the simulations, the efficiency of a single antenna can be expected to be around 80%.

V. CONCLUSION

This letter introduced a new feeding structure for DRAs consisting of differential wideband monopoles, enabling a hybrid operation in slot and DRA mode. Hence, a very wideband exceeding 40% was achieved, which is a good result compared to other works presented in Table III. Additionally, this feeding network facilitates the design of dual-polarized antenna elements using only two metal layers of a standard PCB process. Thus, number of used metal layers could be reduced compared to [7]–[9]. Two prototypes, one of a single DRA and one of a 2×2 DRA array, were fabricated using a standard PCB process and 3-D printing for fabrication of dielectric resonators. The maximal measured gain of a single element is 7.1 dBi, while the array achieves up to 10.4 dBi gain.

REFERENCES

[1] A. Ghosh, A. Maeder, M. Baker, and D. Chandramouli, "5G evolution: A view on 5G cellular technology beyond 3GPP release 15," *IEEE Access*, vol. 7, pp. 127639–127651, 2019.

[2] European Telecommunications Standards Institute (ETSI), *5G; NR; User Equipment (UE) Radio Transmission and Reception; Part 2: Range 2 Standalone (3GPP TS 38.101-2 Version 15.2.0 Release 15)*, ETSI TS 138 101-2, V15.2.0 (2018-07), Reference: RTS/TSGR-0438101-2vf20, Jul. 2018

[3] T. E. Bogale and L. B. Le, "Massive MIMO and mmWave for 5G wireless HetNet: Potential benefits and challenges," *IEEE Veh. Technol. Mag.*, vol. 11, no. 1, pp. 64–75, Mar. 2016.

[4] S. Shinjo, K. Nakatani, K. Tsutsumi, and H. Nakamizo, "Integrating the front end: A highly integrated RF front end for high-SHF wide-band massive MIMO in 5G," *IEEE Microw. Mag.*, vol. 18, no. 5, pp. 31–40, Jul./Aug. 2017.

[5] K. Kibaroglu, M. Sayginer, and G. M. Rebeiz, "A low-cost scalable 32-element 28 GHz phased array transceiver for 5G communication links based on a 2×2 beamformer flip-chip unit cell," *IEEE J. Solid-State Circuits*, vol. 53, no. 5, pp. 1260–1274, May 2018.

[6] Y. Zhang, Z. N. Chen, X. Qing, and W. Hong, "Wideband millimeter-wave substrate integrated waveguide slotted narrow-wall fed cavity antennas," *IEEE Trans. Antennas Propag.*, vol. 59, no. 5, pp. 1488–1496, May 2011.

[7] M. Khalily, R. Tafazolli, P. Xiao, and A. A. Kishk, "Broadband mm-Wave microstrip array antenna with improved radiation characteristics for different 5G applications," *IEEE Trans. Antennas Propag.*, vol. 66, no. 9, pp. 4641–4647, Sep. 2018.

[8] B. Rohrdantz, T. Jaschke, F. K. H. Gellersen, A. Sieganschin, and A. F. Jacob, "Ka-band antenna arrays with dual-frequency and dual-polarized patch elements," *Int. J. Microw. Wireless Technol.*, vol. 8, no. 06, pp. 963–972, Sep. 2016.

[9] C. Chu, J. Zhu, S. Liao, A. Zhu, and Q. Xue, "28/38 GHz dual-band dual-polarized highly isolated antenna for 5G phased array applications," in *Proc. IEEE MTT-S Int. Wireless Symp.*, Guangzhou, China, 2019, pp. 1–3.

[10] R. S. Yaduvanshi and H. Parthasarathy, *Rectangular Dielectric Resonator Antennas*. New Delhi, India: Springer, 2016.

[11] K. Khoo, Y. Guo and L. C. Ong, "Wideband circularly polarized dielectric resonator antenna," *IEEE Trans. Antennas Propag.*, vol. 55, no. 7, pp. 1929–1932, Jul. 2007.

[12] Y. Pan and K. W. Leung, "Wideband circularly polarized trapezoidal dielectric resonator antenna," *IEEE Antennas Wireless Propag. Lett.*, vol. 9, pp. 588–591, 2010.

[13] M. Khalily, M. K. A. Rahim, and A. A. Kishk, "Planar wideband circularly polarized antenna design with rectangular ring dielectric resonator and parasitic printed loops," *IEEE Antennas Wireless Propag. Lett.*, vol. 11, pp. 905–908, 2012.

[14] S. K. Podilchak, J. C. Johnstone, M. Caillet, M. Clénet, and Y. M. M. Antar, "A compact wideband dielectric resonator antenna with a meandered slot ring and cavity backing," *IEEE Antennas Wireless Propag. Lett.*, vol. 15, pp. 909–913, 2016.

[15] Y. X. Sun and K. W. Leung, "Dual-band and wideband dual-polarized cylindrical dielectric resonator antennas," *IEEE Antennas Wireless Propag. Lett.*, vol. 12, pp. 384–387, 2013.

[16] R. D. Gupta and M. S. Parihar, "Differentially fed wideband rectangular DRA with high gain using short horn," *IEEE Antennas Wireless Propag. Lett.*, vol. 16, pp. 1804–1807, 2017.

[17] S. Guo, L. Wu, K. W. Leung, and J. Mao, "Microstrip-fed differential dielectric resonator antenna and array," *IEEE Antennas Wireless Propag. Lett.*, vol. 17, no. 9, pp. 1736–1739, Sep. 2018.

[18] C.-Y. Huang, T.-W. Chiou, and K.-L. Wong, "Dual-polarized dielectric resonator antennas," *Microw. Opt. Technol. Lett.*, vol. 31, pp. 222–223, 2001.

[19] X.-R. Tang, S.-S. Zhong, L.-B. Kuang, and Z. Sun, "Dual-polarised dielectric resonator antenna with high isolation and low cross-polarisation," *Electron. Lett.*, vol. 45, no. 14, pp. 719–720, Jul. 2009.

[20] G. Adamiuk, T. Zwick, and W. Wiesbeck, "UWB antennas for communication systems," *Proc. IEEE*, vol. 100, no. 7, pp. 2308–2321, Jul. 2012.

[21] K. M. Luk and K. W. Leung, *Dielectric Resonator Antennas*, Baldock, U.K.: Research Studies Press, 2003.